RESEARCH ARTICLE

Mutations in the *Borrelia burgdorferi* Flagellar Type III Secretion System Genes *fliH* and *fliI* Profoundly Affect Spirochete Flagellar Assembly, Morphology, Motility, Structure, and Cell Division

Tao Lin,[a] Lihui Gao,[a] Xiaowei Zhao,[a] Jun Liu,[a,b] Steven J. Norris[a,b]

Department of Pathology and Laboratory Medicine[a] and Department of Microbiology and Molecular Genetics,[b] Medical School, University of Texas Health Science Center at Houston, Houston, Texas, USA

ABSTRACT **The Lyme disease spirochete *Borrelia burgdorferi* migrates to distant sites in the tick vectors and mammalian hosts through robust motility and chemotaxis activities. FliH and FliI are two cytoplasmic proteins that play important roles in the type III secretion system (T3SS)-mediated export and assembly of flagellar structural proteins. However, detailed analyses of the roles of FliH and FliI in *B. burgdorferi* have not been reported. In this study, *fliH* and *fliI* transposon mutants were utilized to dissect the mechanism of the *Borrelia* type III secretion system. The *fliH* and *fliI* mutants exhibited rod-shaped or string-like morphology, greatly reduced motility, division defects (resulting in elongated organisms with incomplete division points), and noninfectivity in mice by needle inoculation. Mutants in *fliH* and *fliI* were incapable of translational motion in 1% methylcellulose or soft agar. Inactivation of either *fliH* or *fliI* resulted in the loss of the FliH-FliI complex from otherwise intact flagellar motors, as determined by cryo-electron tomography (cryo-ET). Flagellar assemblies were still present in the mutant cells, albeit in lower numbers than in wild-type cells and with truncated flagella. Genetic complementation of *fliH* and *fliI* mutants in *trans* restored their wild-type morphology, motility, and flagellar motor structure; however, full-length flagella and infectivity were not recovered in these complemented mutants. Based on these results, disruption of either *fliH* or *fliI* in *B. burgdorferi* results in a severe defect in flagellar structure and function and cell division but does not completely block the export and assembly of flagellar hook and filament proteins.**

IMPORTANCE **Many bacteria are able to rapidly transport themselves through their surroundings using specialized organelles called flagella. In spiral-shaped organisms called spirochetes, flagella act like inboard motors and give the bacteria the ability to bore their way through dense materials (such as human tissue) in a corkscrew manner. In this article, we studied how two proteins, called FliH and FliI, are important for the production of full-length flagella in the Lyme disease spirochete *Borrelia burgdorferi*. Mutants with defective production of FliH and FliI have reduced flagellar length and motility; this deficiency in turn affects many aspects of *B. burgdorferi*'s biology, including the ability to undergo cell division and cause disease in mammals. Using a microscopic computed tomography (CT) scan approach called cryo-electron tomography, the structure that contains FliH and FliI was defined in the context of the flagellar motor, providing clues regarding how this amazing nanomachine is assembled and functions.**

Received 7 April 2015 **Accepted** 16 April 2015 **Published** 12 May 2015

Citation Lin T, Gao L, Zhao X, Liu J, Norris SJ. 2015. Mutations in the *Borrelia burgdorferi* flagellar type III secretion system genes *fliH* and *fliI* profoundly affect spirochete flagellar assembly, morphology, motility, structure, and cell division. mBio 6(3):e00579-15. doi:10.1128/mBio.00579-15.

Editor Alan G. Barbour, University of California Irvine

Address correspondence to Tao Lin, Tao.Lin@uth.tmc.edu.

T.L., L.G., and X.Z. contributed equally to this work.

This article is a direct contribution from a Fellow of the American Academy of Microbiology.

Lyme disease is the most commonly reported arthropod-borne illness in the United States and Eurasia and continues to expand in both incidence and geographic distribution. It is a multistage, systemic infection caused by at least three pathogenic genospecies of the *Borrelia burgdorferi* sensu lato complex, including *B. burgdorferi* sensu stricto in North America and *Borrelia garinii*, *Borrelia afzelii*, and *B. burgdorferi* sensu stricto in Eurasia (1, 2). Lyme disease *Borrelia* strains are transmitted to humans via the bite of infected ticks of the *Ixodes ricinus* group (3). This highly motile and invasive spirochete is an obligate parasite in both ticks and mammals but produces no known toxins. The organism can invade almost any tissue, evades the immune system in infected humans and animals through gene downregulation, antigenic variation, and complement inactivation, and establishes persistent infection that induces inflammatory responses and tissue damage in multiple organs and tissues (4). Symptoms include erythema migrans and malaise in the localized infection stage, followed by neurologic, arthritic, and cardiologic manifestations during the disseminated and persistent stages of infection (1, 5, 6).

B. burgdorferi is a highly motile and invasive spirochete with 7 to 11 periplasmic flagella (PFs) subterminally attached to the linearly arranged flagellar motors at each end of the protoplasmic cell

cylinder (7, 8). The flagellar filaments form flat ribbons wrapping around the peptidoglycan layer in a right-handed helix (9). The flagellar assemblies of *B. burgdorferi* and other spirochetes have an overall structure and protein composition similar to those found in other bacteria (10–19). However, certain differences exist in the PFs of spirochetes, including the presence of (i) a unique periplasmic collar structure associated with the rotor, (ii) multiple homologous flagellar filament proteins (FlaB) in *Treponema*, *Leptospira*, *Serpulina*, and *Spirochaeta* species, and (iii) a flagellar sheath protein (FlaA) (8, 16). The PFs are essential for the flat wave morphology, unique motility, and infectivity of *B. burgdorferi* (7, 8, 20–24).

The bacterial flagellum is composed of at least 30 proteins and consists of three major parts: the basal body, the hook, and the filament; the basal body, which constitutes the rotary motor, is further subdivided into the rotor (including the MS ring, rod, C ring, P ring, and L ring) and the stator (17, 18, 25). Many of the flagellar structural proteins (including those comprising the rod, hook, and filament) are exported across the cytoplasmic membrane by the flagellar protein export apparatus, also called the flagellar type III secretion system (fT3SS) family (26–28). Virulence-associated members of type III secretion family (vT3SS) produced by certain Gram-negative bacteria are specialized for the transfer of effector proteins into host cells (29).

In *Salmonella enterica* serovar Typhimurium and *Escherichia coli*, the fT3SS is comprised of six membrane-embedded proteins (FlhA, FlhB, FliO, FliP, FliQ, and FliR) and three soluble cytoplasmic proteins (FlIH, FliI, and FliJ) (17, 18, 25, 30); this assembly was the subject of a recent comprehensive review by Minamino (26). The integral membrane proteins form a proton-driven export gate within the central pore of the MS ring (28, 31) and the soluble components form a complex to bind and deliver export substrates to the export gate (28, 31, 32). The exported flagellar proteins are synthesized in the cytoplasm and then escorted and delivered to the export gate by a complex formed by ATPase FliI and its negative regulator FliH with the help of the flagellum-specific chaperone FliJ (18, 33, 34). FliI is a member of the Walker-type ATPase family (35) and is similar in sequence and structure to α and β subunits of F_oF_1-ATP synthase (36–39). It self-assembles into a ring-shaped hexamer in the cytoplasm to exert its ATPase activity (40). The FliI ATPase is required for efficient flagellar protein export (33, 34, 36, 39), although defective flagellar assembly in Δ*fliHI Salmonella* Typhimurium mutants can be partially overcome by increasing the proton motive force (PMF) (41). FliI interacts with FliH and FliJ, and its ATPase activity is suppressed by FliH (18, 37, 42–45). FliH promotes the docking of FliI onto the platform (45). Several residues of *Salmonella* Typhimurium FliH are required for interaction with FliI (residues 100 to 235), FliH dimerization (residues 101 to 141), and binding to the enterobacterial flagellar chaperone FliJ N-terminal residues (46). In addition, residues 60 to 100 of FliH appear important for inhibition of FliI ATPase activity. FliJ has several activities, including promotion of FliI hexamer ring formation and efficient flagellar protein export (28, 42, 47), interaction with export substrates, prevention of their premature aggregation in the cytoplasm (48), and facilitation of export substrate delivery to the export gate by binding to the linker region of the C-terminal cytoplasmic domain of FlhA (FlhAc) (47–49). Additional chaperone proteins, such as FliT and FlgN, are also involved in this process (50, 51). The export gate complex utilizes PMF to translocate the flagellar proteins across the cytoplasmic membrane through a port in the nascent flagellar motor (28, 31). ATP is utilized in the dissociation of the FliH-FliI-FliJ complex and unfolding of substrates (18). The substrate specificity of the export apparatus is well regulated by a highly ordered flagellar assembly process in the cell exterior (18).

Relatively little is known about the structure and function of the flagellar export apparatus of *B. burgdorferi* and other spirochetes. As part of an overall goal to dissect the mechanisms of *Borrelia* chemotaxis and motility and their relationship to pathogenesis, we selected *fliH* and *fliI* transposon mutants from a sequence-defined transposon library (22) for further study. The effects of mutation of *fliH* and *fliI* on the morphology, motility, swimming ability, growth and cell division, flagellar motor structure, and infectivity were determined. Genetic complementation of *fliH* and *fliI* mutants was performed to confirm the phenotypes. Additional information regarding the *B. burgdorferi* flagellar protein export apparatus and its role in the biology of the organism was revealed. The results were compared to those in a recent study by Guyard et al. (23), in which the effects of a spontaneous 142-bp deletion in *fliH* of the relapsing fever organism *Borrelia hermsii* were analyzed.

RESULTS

Initial characterization and complementation of *fliH* and *fliI* mutants. To investigate the structure and function of the *B. burgdorferi* flagellar type III secretion system and its role in assembly of flagella and pathogenesis of Lyme disease spirochetes, we constructed *fliH* and *fliI* transposon mutants in the infectious *B. burgdorferi* strain 5A18NP1 using a signature-tagged mutagenesis (STM) system (Table 1). For simplicity, 5A18NP1, the *fliH* mutant T05TC243, and the *fliI* mutant T10TC091 will be referred to as the wild-type (WT), *fliH*::Tn, and *fliI*::Tn strains, respectively, in this article. The *fliH* mutant was characterized using reverse transcriptase PCR (RT-PCR), and transposon insertions did not exhibit an obvious polar effect on expression of downstream genes *fliI* and *fliJ* (see Fig. S1 in the supplemental material); the high *fliI* transcript levels in the complemented mutant are discussed in a subsequent section. Both *fliH*::Tn and *fliI*::Tn mutants have an elongated, rod-shaped or string-like morphology and exhibit reduced, sporadic motion close to the ends of the organisms (Fig. 1; see Movies S2 to S5 in the supplemental material). In early log phase, *B. burgdorferi fliH* and *fliI* mutants showed a rod-shaped morphology with curvature near the cell ends and in the middle of cells at incomplete division points (Fig. 1C and E; see also Movies S2 and S4). In late log phase, the *fliH*::Tn and *fliI*::Tn strains exhibited a more elongated, filamentous morphology (Fig. 1D and F; see Movies S3 and S5). Cryo-electron tomography (cryo-ET) (Fig. 2) revealed that incomplete division points were common and consisted of regions where the cytoplasmic membranes of daughter cells had divided and flagellar motors formed but the outer membrane had not divided. In some cases, the peptidoglycan layer appeared to form around the ends of the cytoplasmic cylinders, but the interconnected daughter cells were separated by a bolus of amorphous material of unknown composition. The microscopy results indicate that spirochetal motility facilitates the separation of daughter cells, and the incomplete flagellar biosynthesis and defective motility of the *fliH* and *fliI* mutants result in incomplete cell separation.

As expected, the defect in cell division in these mutants resulted in delayed increases in cell numbers (see Fig. S2). The mean generation times or doubling times for the WT and the *fliH* and *fliI*

TABLE 1 Phenotypes of *Borrelia burgdorferi* parental strain, *fliH* and *fliI* mutants, and complemented clones

Clone	Genotype	Plasmids missing	Brief name	Morphology	Motility	Swarming Ability	Cell division	Structure	Reference
5A18NP1[a]	BBE02::Kan^r lp28-4$^-$ lp56$^-$	lp28-4, lp56	WT	Helical	Motile	+	Normal	WT FliH-FliI complex and flagella	61
T05TC243[b]	5A18NP1 BB0289::Tn (Gen^r)	lp5, lp28-4, lp56	*fliH*::Tn mutant	Predominantly linear, elongated	Weak motility	−	Defective	Fewer motors, missing FliH-FliI complex, absent or truncated flagella	22
T10TC091[c]	5A18NP1 BB0288::Tn (Gen^r)	lp5, lp28-2, lp28-4, lp56	*fliI*::Tn mutant	Predominantly linear, elongated	Weak motility	−	Defective	Fewer motors, missing FliH-FliI complex, absent or truncated flagella	22
LGPH1	5A18NP1/pKFFS1::*pflaBfliH*	cp9, lp5, lp28-4, lp56	WT/p*fliH*	Helical	Motile	ND[d]	Normal	ND	This study
LGHH9	T05TC243/pKFFS1::*pflaBfliH*	cp9, cp32-6, lp5, lp28-4, lp56	*fliH*::Tn/p*fliH* mutant	Helical	Motile	ND	Normal	WT FliH-FliI complex, flagella shorter than WT	This study
LGHHI8	T05TC243/pKFFS1::*pflaBfliHI*	cp9, cp32-4, lp5, lp28-4, lp56	*fliH*::Tn/p*fliHI* mutant	Helical	Motile	±	Normal	WT FliH-FliI complex, flagella shorter than WT	This study
LGII51	T10TC091/pKFFS1::*pflaBfliI*	cp9, lp5, lp28-2, lp28-4, lp56	*fliI*::Tn/p*fliI* mutant	Helical	Motile	ND	Normal	WT FliH-FliI complex, flagella shorter than WT	This study
LGIHI6	T10TC091/pKFFS1::*pflaBfliHI*	cp9, lp5, lp28-2, lp28-4, lp56	*fliI*::Tn/p*fliHI* mutant	Helical	Motile	ND	Normal	WT FliH-FliI complex, flagella shorter than WT	This study

[a] Genetic modified *B. burgdorferi* B31 clone in which lp28-4 and lp56 have been lost and bbe02 on lp25 has been inactivated.

[b] fliH transposon mutant, *fliH* gene is inactivated by insertion of transposon, insertion site = 299448 in chromosome, insertion ratio = 0.29 [nucleotides(beginning of the open reading frame to the transposon insertion site)/nucleotides(open reading frame)].

[c] fliI transposon mutant, *fliI* gene is inactivated by insertion of transposon, insertion site = 297745 in chromosome, insertion ratio = 0.79.

[d] ND, not determined.

mutant cells were 8.05, 10.21, and 9.58 h, respectively. Remarkably, vigorous vortexing for 30 s resulted in separation of many of the longer cells with incomplete division points, yielding a higher proportion of cells with lengths in the WT range. The cells remained motile afterward, indicating that viability was maintained through this process.

To confirm the correlation of observed phenotypes of *fliH* and *fliI* mutants with the gene disruptions, we performed genetic complementation in *trans* using the shuttle vector pKFSS1 (52). Three constructs were utilized, including *fliH* alone, *fliI* alone, and *fliHI* together in their native configuration; in each case, the promoter for the *flaB* flagellar filament gene was used to drive transcription. These constructs are referred to as p*fliH*, p*fliI*, and p*fliHI* in this article. In *trans* complementation of *fliH*::Tn (with *fliH* or *fliHI* constructs) or *fliI*::Tn (with *fliI* or *fliHI*) strains restored the spiral appearance and characteristic motility of the organisms (Fig. 3; see also Movie S2 in the supplemental material). Quantitative RT-PCR (qRT-PCR) results (see Fig. S1) indicated that complementation with p*fliHI* resulted in an *fliI* transcript level ~10-fold higher than the WT level, most likely because of the use of the strong *flaB* promoter in the complementation constructs. *fliH* transcript levels were not tested but are expected to be similar.

Dark-field microscopy combined with video analysis of the WT parental clone, *fliH* and *fliI* mutants, and complemented *fliH* and *fliI* mutants was performed in Barbour-Stoenner-Kelly II (BSKII) medium with and without the viscosity agent methylcellulose to examine motility in greater detail. As expected, WT *B. burgdorferi* cells in BSKII medium ran, flexed, and reversed (see Movie S1) and exhibited increased translational motion in the presence of 1% methylcellulose. However, the *fliH* and *fliI* mutants exhibited sporadic, uncoordinated movement near the cell ends and near apparent incomplete division points (see Movies S2 and S4) and had substantially less swimming ability in 1% methylcellulose compared to WT cells. In late log phase, the cells became highly elongated and exhibited only slight movement at the ends (see Movies S3 and S5). Genetic complementation of *fliH* and *fliI* mutants in *trans* with either single gene or *fliHI* constructs restored wild-type motility and swimming ability in both BSKII medium and BSKII medium containing 1% methylcellulose (Table 1; see also Movie S2).

Behavior of mutants and complemented mutants in swarm plate assay. Swarm plate assays were performed to compare the ability of WT organisms, *fliH* and *fliI* mutants, and complemented mutants to translocate in low-percentage agarose matrices. Whereas the visible "halo" of the parental clone 5A18NP1 had a diameter of ~12 mm in 0.25% agarose at 5 days, the *fliH* and *fliI* mutants migrated only a short distance from the inoculation well (Fig. 4A). Complementation of the *fliH*::Tn mutant with *fliHI* in *trans* resulted in a swarm diameter comparable to that of the 5A18NP1 parent in 0.25% agarose (Fig. 4B). In the presence of a relatively dense 0.34% agarose matrix, the migration diameter of the WT parent was reduced from 12.3 mm to 7.0 mm (Fig. 4C and D). In addition, the swarm diameter of the complemented mutant was significantly smaller than that of the parent strain in the presence of 0.34% agarose ($P < 0.003$). These results indicate that the ability of the complemented mutant to translocate in agarose matrices is not restored completely in the complemented mutant.

Effects of *fliH* or *fliI* mutation on flagellar motor and filament structure. The molecular architecture of the flagellar motor in the *fliH* and *fliI* mutants and their complemented derivatives

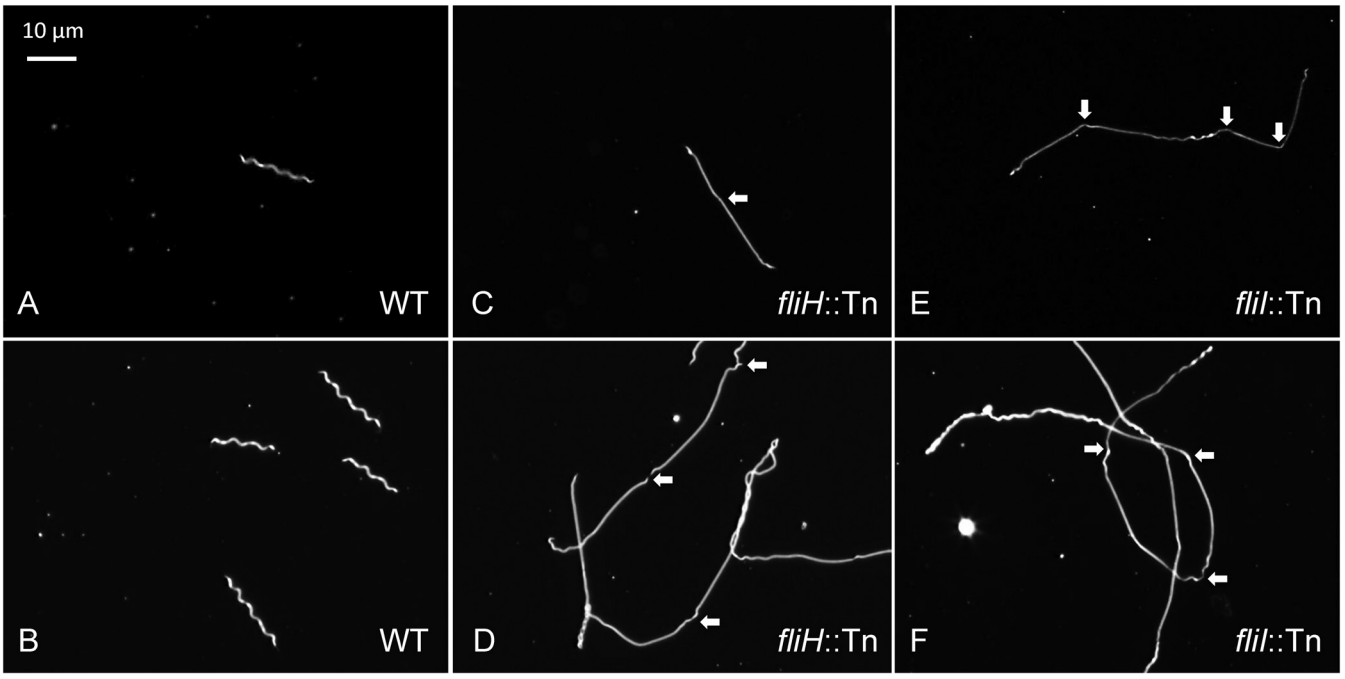

FIG 1 Micrographs of wild-type *B. burgdorferi* clone 5A18NP1 (WT), *fliH* mutant (*fliH*::Tn), and *fliI* mutant (*fliI*::Tn) observed in different growth phases. The WT (A and B), *fliH*::Tn mutant (C and D), and *fliI*::Tn mutant (E and F) are shown in early log phase (top) and late log phase (bottom). While no obvious morphology defects were observed in WT organisms, both the *fliH* mutant and the *fliI* mutant exhibited extreme cellular elongation with incomplete division points (arrows), most having curvature indicative of partial flagellar assembly.

were determined by cryo-ET and subvolume averaging. The motor subvolumes ($n = 277$ to 590 for each genotype) were extracted from a total of 303 tomograms of *fliH* and *fliI* mutants and complemented mutants (see Table S1 in the supplemental material) and then used to generate three-dimensional (3D) flagellar motor structures at a resolution of ~4 nm; these were compared to the previously determined WT flagellar motor structure (12). Cryo-ET results indicated that profound differences were present in the secretory apparatus of the flagellar motor of the *fliH* and *fliI* mutants in comparison to the parental clone and complemented mutants (Fig. 5). In WT organisms, FliH and FliI are predicted to form a complex inside the C ring just under a torus-shaped complex comprised of the C-terminal portion of FlhA (Fig. 5C, F, and I). Both *fliH* (Fig. 5D and J) and *fliI* (Fig. 5G) mutants lacked densities corresponding to the FliH-FliI complex, although the presumed FlhAc-associated density remained intact. Complementation of *fliH* or *fliI* (Fig. 5E, K, and H) resulted in restoration of the density attributed to the FliH-FliI complex. Thus, the assembly of this complex is dependent upon the presence of both components.

In addition to the observed loss of the FliH/FliI-associated densities in the *fliH* and *fliI* mutants, both mutants exhibited ~25% fewer flagellar motors per cell end and also had shorter flagella (Fig. 6) than the WT cells. The number of motors was restored to near WT levels in the complemented mutants (Fig. 6I). We also noted that the flagella in the mutant strains tended to be shorter than in the WT. To further assess this phenomenon, high-dose cryo-electron micrographs were taken along the length of cells from *fliH* and *fliI* mutants, complemented mutants, and the parental clone 5A18NP1. Examples of cryo-electron microscopy (cryo-EM) images of WT and *fliI* mutant cells are provided in Fig. 6A to H. As observed previously, the parental clone exhibited flagellar ribbons with ~8 full-length flagella that extended through the tip and subcentral and central regions of the cells (Fig. 5, 6). In contrast, the *fliH*, *fliI*, and complemented mutants all exhibited short flagella that were <1 μm long (ranging from 12% to 23% of the total number of flagella); no truncated flagella were observed in the 13 WT cells examined. In addition, the lengths of nearly all of the flagellar filaments were shortened in *fliH* and *fliI* mutants, as indicated by the histograms in Fig. 6J (*fliH* mutant) and Fig. 6K (*fliI* mutant). While complementation of *fliH*::Tn cells resulted in nearly complete restoration of flagellar length, *fliI*::Tn complementation yielded only partial restoration (Fig. 6J and K). Consistent with the shorter flagellar length, the *fliH*::Tn and *fliI*::Tn mutants exhibited a decrease in FlaB concentrations, whereas FlaB level was restored by complementation of FliH expression in the *fliH*::Tn mutant (see Fig. S3).

Infectivity studies. Previously reported STM studies provided the first indication that FliH and FliI are critical for infection of the immunocompetent C3H/HeN mice (22). To confirm the STM results, groups of six C3H/HeN mice were inoculated subcutaneously with 10^5 cells of the parental 5A18NP1 clone, the *fliH* mutant, or the *fliI* mutant. Blood specimens were collected at day 7 postinoculation, and three mice from each group were sacrificed at days 14 and 28 postinoculation, and skin, tibiotarsal joint, heart, and urinary bladder were collected for culture of spirochetes. None of the cultures from mice inoculated with *fliH* or *fliI* mutants yielded *B. burgdorferi*, whereas all cultures from mice inoculated with the parental strain 5A18NP1 were positive. Genetic complementation of *fliH* and *fliI* mutants in *trans* did not restore infectivity, most likely due to the incomplete complementation of flagellar filament assembly and motility in dense matrices in these mutants, as described above.

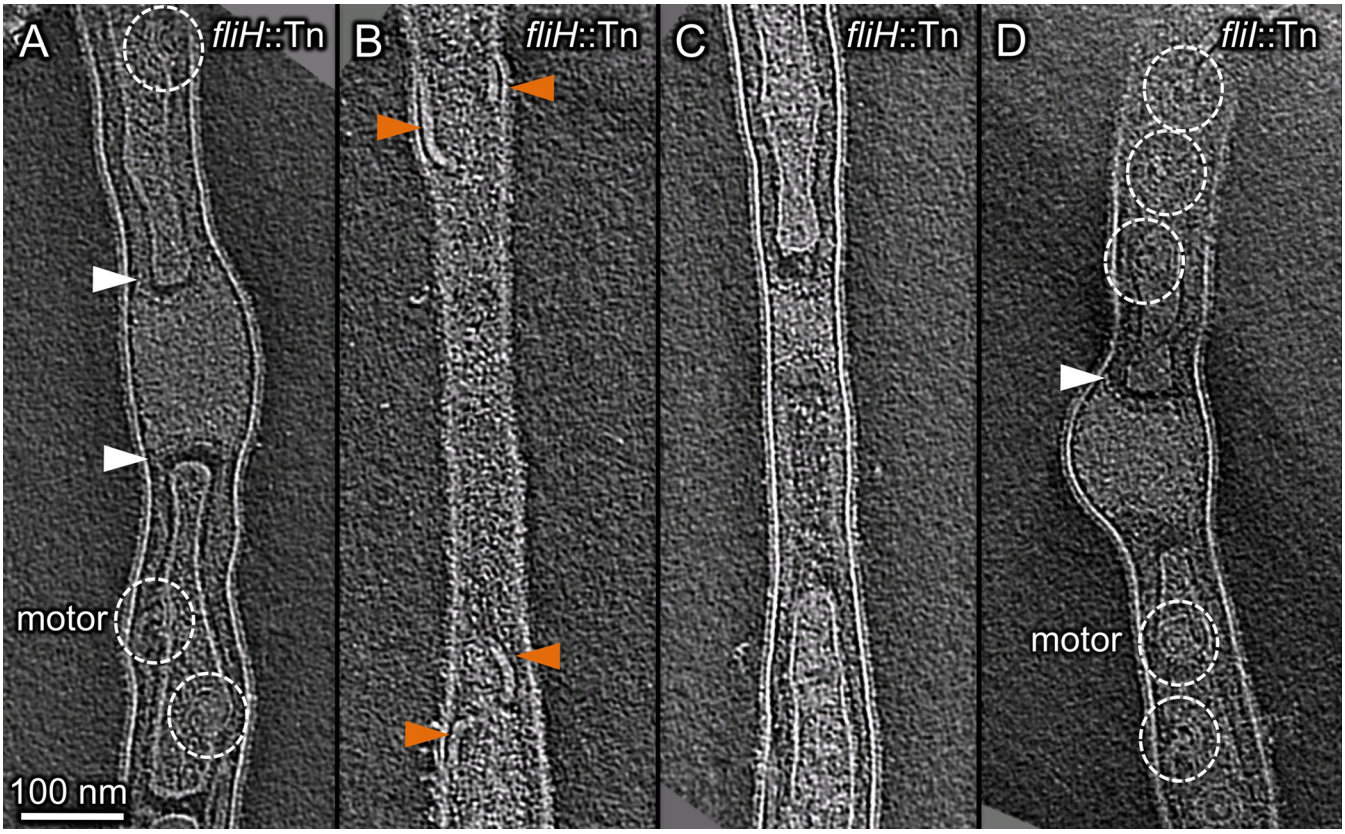

FIG 2 Cryo-ET images of *B. burgdorferi fliH*::Tn and *fliI*::Tn mutants, showing incomplete division points and other cellular features. Incomplete division points were commonly present in both *fliH*::Tn (A to C) and *fliI*::Tn (D) mutants. The cytoplasmic membranes of daughter cells had clearly separated, and in some instances apparent formation of a peptidoglycan layer around the end of the cytoplasmic membrane was visible (white arrowheads). Flagellar motors had formed at the division points (dashed circles), and some flagella are truncated (orange arrowheads).

DISCUSSION

Disruption of either *fliH* or *fliI* had profound effects on *B. burgdorferi* cellular morphology, motility, flagellar motor and filament structure, and cell division. At the ultrastructural level, cryo-ET revealed that inactivation of either *fliH* or *fliI* resulted in the loss of densities associated with both protein products, indicating that the presence of both proteins is required for the stable formation of an FliH-FliI complex at the cytoplasmic apex of the secretion apparatus. Surprisingly, the absence of either FliH or FliI did not prevent assembly of the remainder of the flagellar motor, although the number of motors did decrease from the WT level of approximately 8 to about 6 per cell pole. Flagellar filaments were also present on most motors, although with decreased lengths; the filaments appeared to be truncated at the hook level in approximately 10% of the motors. In other bacteria, the ATPase FliI facilitates the delivery of export substrates to the secretory apparatus, while FliH is involved in the positioning of FliI near the export channel (33, 44, 46, 53). Our results indicate that, in *B. burgdorferi*, FliH and FliI are not required for uptake of protein substrates by the export apparatus; thus, their absence does not prevent the formation of flagellar motors and filaments. However, export of the FlaB filament protein is much less efficient, resulting in shorter filaments. These results are comparable to those obtained by Erhardt et al. with *Salmonella* Typhimurium (41). In their studies, flagellar filament assembly and swimming motility were minimal in *fliH* and *fliI* mutants but could be increased by mutations or culture conditions that increased either flagellar protein expression or the PMF, thereby raising the substrate levels or the available energy gradient for export. It is possible that the export system by itself can transport the proteins at a low rate, or that other chaperone systems may facilitate this process. Nevertheless, the decreased efficiency of substrate delivery in *B. burgdorferi* mutants results in defective motility and a crippled organism that does not divide efficiently.

Studies in other organisms have firmly established that the ATPase FliI forms a hexameric ring and associates with both FliH dimers and FliJ to form the ATPase complex in the cytoplasm near the export apparatus (33, 44, 46, 53). Furthermore, FliH interacts with C ring protein FliN (54, 55). In some models, the ATPase complex has two alternative associations with the flagellar motor, one with the C ring and the other in close proximity to the export apparatus (54, 55). Our cryo-ET analyses of *B. burgdorferi* indicate that FliH and FliI form a stable complex directly below the export apparatus (Fig. 5). The *fliH*::Tn and *fliI*::Tn mutants lack a discernible density in this region, consistent with a requirement that both proteins must be present in order for a stable association to occur. In a companion article on the export apparatus (J. Tu, X. Zhao, A. Manne, K. Lees, A. Yerke, K. Zhang, C. Li, S. J. Norris, M. A. Motaleb, and J. Liu, submitted for publication), high-resolution cryo-ET reconstructions of the WT *B. burgdorferi* fla-

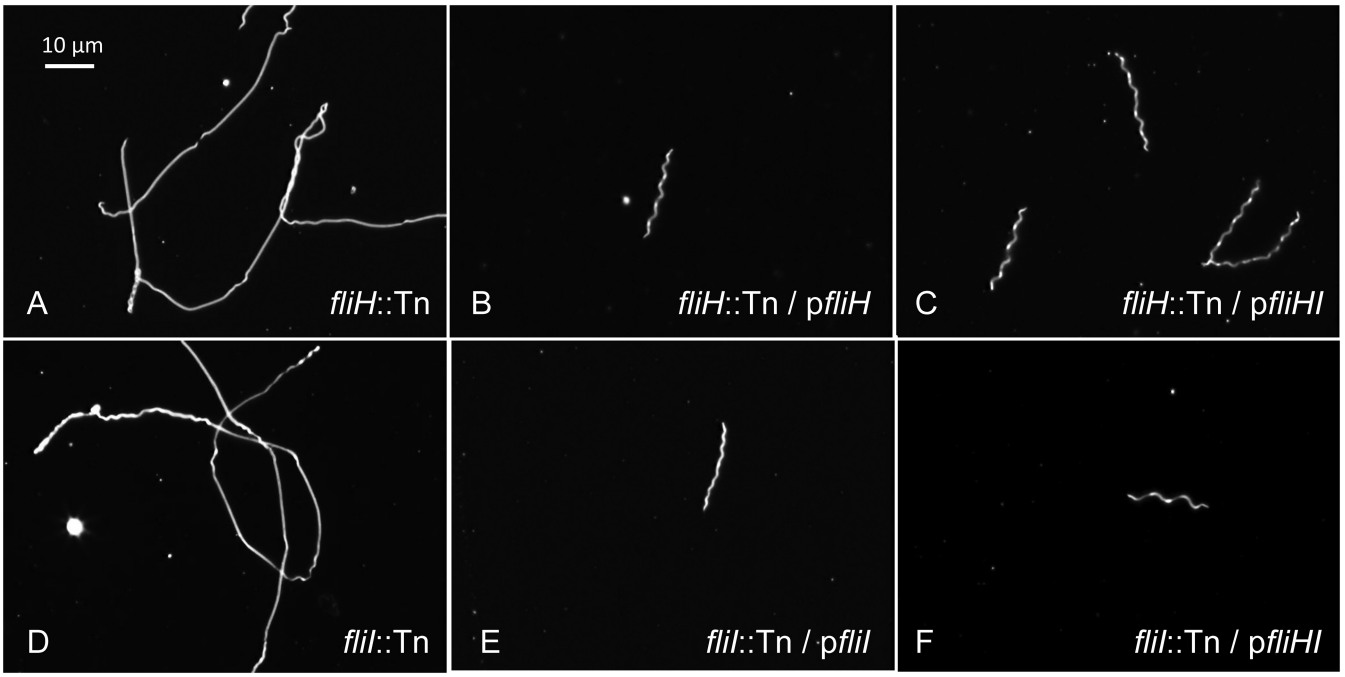

FIG 3 Complementation in *trans* using recombinant plasmids for *fliH* (p*fliH*), *fliI* (p*fliI*), or both *fliH* and *fliI* (p*fliHI*) restores *B. burgdorferi fliH* and *fliI* mutants to near wild-type morphology. Micrographs of the following cell types are shown: *fliH*::Tn mutant (A), *fliH*::Tn/p*fliH* mutant (B), *fliH*::Tn/p*fliHI* mutant (C), *fliI*::Tn mutant (D), *fliI*::Tn/p*fliI* mutant (E), and *fliI*::Tn/p*fliHI* mutant (F).

gellar motor revealed that elongated, propeller-shaped densities extend from the central FliI hexamer to the C ring. Our current model is that six FliH dimers form a scaffold that tethers FliI in its central location and that this structure is further stabilized by the interaction of FliJ with both FliI and FlhA (42, 49).

The qualitative decrease in flagellar function in *fliH* and *fliI* mutants was manifested in several ways, including a weakened motility and altered morphology. By dark-field microscopy, helical morphology was observed near the ends of the spirochetes. However, the organisms exhibited straight regions toward the middle of the cells, particularly in the elongated forms. This result is consistent with the cryo-EM observation that flagella, although present in the *fliH* and *fliI* mutants, were shortened and found in reduced numbers. Absence of periplasmic flagella in *B. burgdorferi* mutants of the flagellar filament protein gene *flaB* results in straight, elongated organisms (7, 8, 20–24), indicating that the flagella (which themselves have an inherent helical shape) are required for the spiral shape of WT cells. Thus, the reduced numbers of flagella near the middle of the *fliH* and *fliI* mutants apparently are unable to exert sufficient force to induce curvature of the cytoplasmic cylinder, suggesting a quantitative effect. The reduced flagellar length and number are also related to the altered motility, in which the ends of the cells in the mutants move sporadically, and greatly elongated cells exhibit little observable motility. Swarm plate analyses indicated that the reduced number and length of flagella, as well as the lengthening of the cells, render the cells unable to migrate effectively through agarose.

The elongated *fliH* and *fliI* mutants also exhibited many incomplete division points (Fig. 2). These regions were characteristically angular, flexible isthmi that often exhibit helical structure and motility, consistent with the presence of flagellar motors and filaments. Indeed, such incomplete division points are commonly observed in WT spirochetes that are about to divide. Although not discussed in detail in prior publications, micrographs of *flaB* mutants exhibit the same angular isthmi, but without the curvature conveyed (in *Borrelia* species) by the flagella (20, 23). Thus, the robust motility observed in WT spirochetes appears to play an important role in the final separation of spirochetal cells, so that defects in motility result in the elongated structures seen in Fig. 1. It is likely that the cytoplasmic membrane (and perhaps the peptidoglycan layer) of neighboring daughter cells has separated, while the outer membrane remained intact. Vortexing was sufficient to separate at least some of these strings of cells during the early stage of growth, and presumably the sheared outer membrane at the end is able to coalesce around the end of the cell, maintaining cell viability. In future studies, we will examine this phenomenon in greater detail.

Although *fliH* and *fliI* mutants continued to assemble flagellar motors and filaments (albeit in reduced numbers and length), infectivity of the organisms in mice was completely abolished. Motility appears to be absolutely required for *B. burgdorferi* infectivity (22, 24, 56), so it is likely that the reduced motility observed in these mutants is sufficient to prevent effective movement through tissue and thus cripple both dissemination and the evasion of accumulating phagocytes. Incomplete cell division may also contribute, although the relatively viscous tissue environment may provide enough resistance to at least partially alleviate this defect. It is of interest that *fliH* and *fliI* mutants are able to survive in the relatively quiescent environment of the tick midgut (22).

Complementation of the mutants in *trans* using vectors expressing either the cognate gene or *fliHI* together was sufficient to restore WT morphology and cell division (Fig. 3), flagellar motor structure (Fig. 5), and the number of motors per cell end (Fig. 6); it also promoted swimming ability in the relatively low agarose

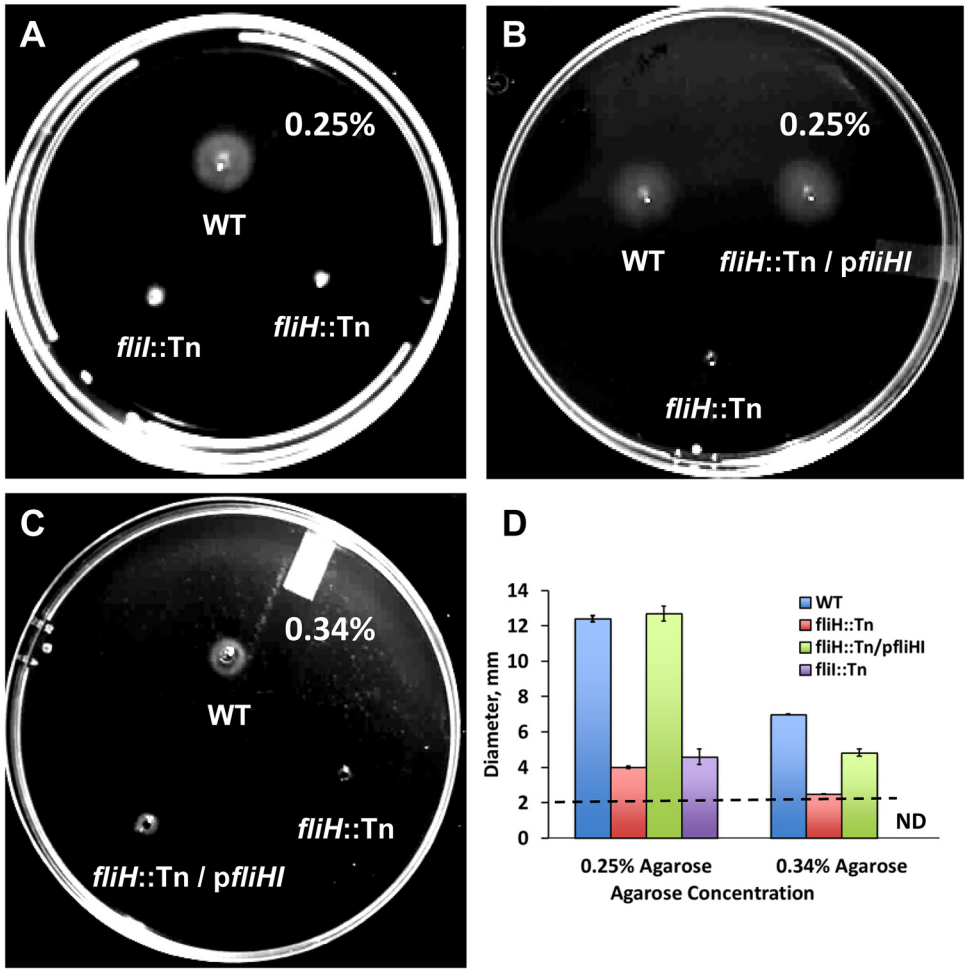

FIG 4 Translational mobility of the WT, *fliH*::Tn mutant, *fliI*::Tn mutant, and the *fliH*::Tn/p*fliHI* complemented mutant in agarose matrices. Motility in 0.25% agarose (A and B) and 0.34% agarose (C) swarm plates was examined. Complementation resulted in full restoration of mobility in 0.25% agarose, but only partial restoration was observed in 0.34% agarose (D). Dashed line indicates the nominal diameter of the inoculation wells. ND, not determined.

concentration of 0.25%. However, the complemented mutants still had shortened flagella, reduced migration in 0.34% agarose (Fig. 4C), and a lack of mouse infectivity. While polar effects of transposon insertion are always a concern, this (see Fig. S1 in the supplemental material) and prior studies (57) indicate that the *Himar1*-based transposon used in these studies does not markedly reduce the transcript levels in downstream genes. Furthermore, the *fliH* and *fliI* mutants exhibited apparently normal assembly of the flagellar motor except for the export apparatus. For example, the C ring, comprised in part by the products of downstream genes *fliM* and *fliN*, is intact in the averaged reconstructions of the *fliH* and *fliI* motors. An alternative explanation is that in *trans* expression results in the translation of the protein products from a different polysome, which may alter the dynamics of assembly of gene products that are typically synthesized in the same cellular microenvironment. In addition, the expression level of the complementing gene from the nonnative *flaB* promoter was roughly 10-fold higher than in WT cells (see Fig. S1), which may interfere with proper assembly. Complementation of the *fliI* mutant was less effective than that in the *fliH* mutant in terms of the length of the flagella (Fig. 6). One could speculate that a nearly full-length protein product could be produced by the *fliI*::Tn mutant T10TC091 (insertion ratio, 0.79) and may interfere with flagellar assembly. Lack of effective complementation in *trans*, particularly with regard to infectivity, has been observed with other *B. burgdorferi* genes (57–59) and continues to be an issue in genetic studies of this organism.

Guyard et al. (23) recently reported a study in which a *B. hermsii* clone with a spontaneous 142-bp deletion in *fliH* was thoroughly characterized. The results that they obtained were similar to our findings with the *B. burgdorferi fliH* and *fliI* mutants, with some differences. The *B. hermsii fliH* mutant cells were nonmotile and straight, and no flagella were detected in 48% of cells by negative-stain EM or cryo-ET; the numbers of flagella were reduced in all mutant cells in comparison to WT cells. The number and structure of the flagellar motors were not examined in the *B. hermsii* study. Cell elongation and the appearance of incomplete division points were not mentioned, although evidence of the latter is apparent in Fig. 5 of the Guyard et al. article (23). Complementation resulted in restoration of infectivity in the *B. hermsii* study (23), although a similar shuttle vector was employed. In contrast, the *B. burgdorferi* fliH and *fliI* mutants always contained some flagella and exhibited weak motility and cell curvature near the ends and at incomplete division points. Elongated

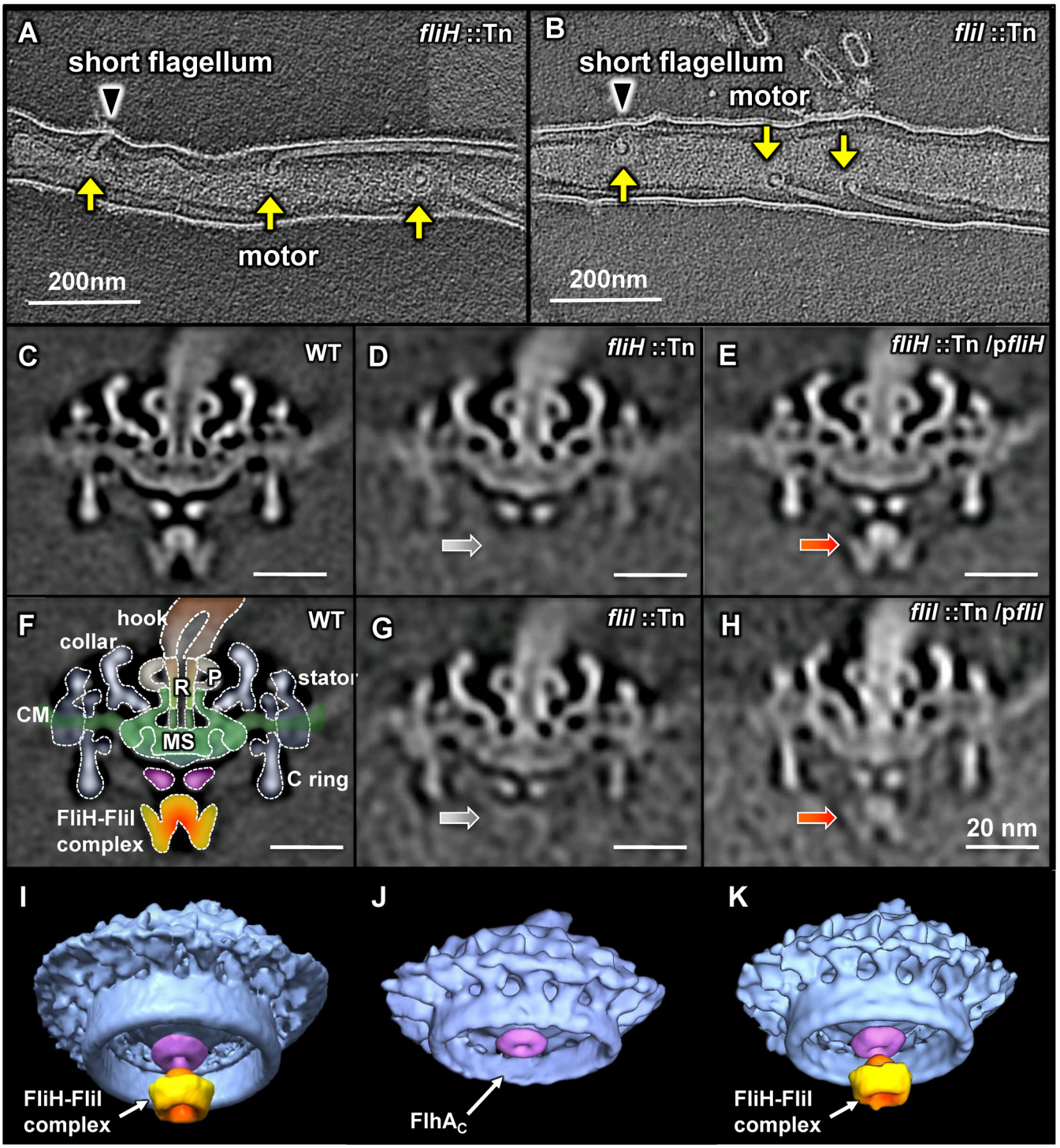

FIG 5 Localization of the flagellar export apparatus proteins FliH and FliI in the *B. burgdorferi* flagellar motor as determined by cryo-ET-derived models from transposon mutants. Panels A and B are cryo-ET sections of *fliH*::Tn and *fliI*::Tn mutant cells. The arrowheads indicate the presence of short flagellar filaments. The yellow arrows indicate flagellar motors. Panels C to H are the central sections from the 3-D averaged reconstructions of flagellar motors from WT cells (C and F), *fliH*::Tn mutant cells (D), *fliI*::Tn mutant cells (G), and complemented clones (E and H). Major flagellar components are outlined in panel F. P, P ring; MS, MS ring; R, rod; CM, cytoplasmic membrane. The cytoplasmic component of the export apparatus is highlighted in red. The cytoplasmic domain of FlhA is colored purple. The gray arrows (in panels D and G) indicate that the densities of the FliH-FliI complex are missing in *fliH* and *fliI* mutants. The red arrows (in panels E and H) indicate the restoration of the FliH-FliI complex in the complemented *fliH* and *fliI* mutants. Panels I to K are the corresponding surface renderings of flagellar motors from the WT (I), *fliH*::Tn mutant (J), and *fliH*::Tn/p*fliH* complemented mutant (K).

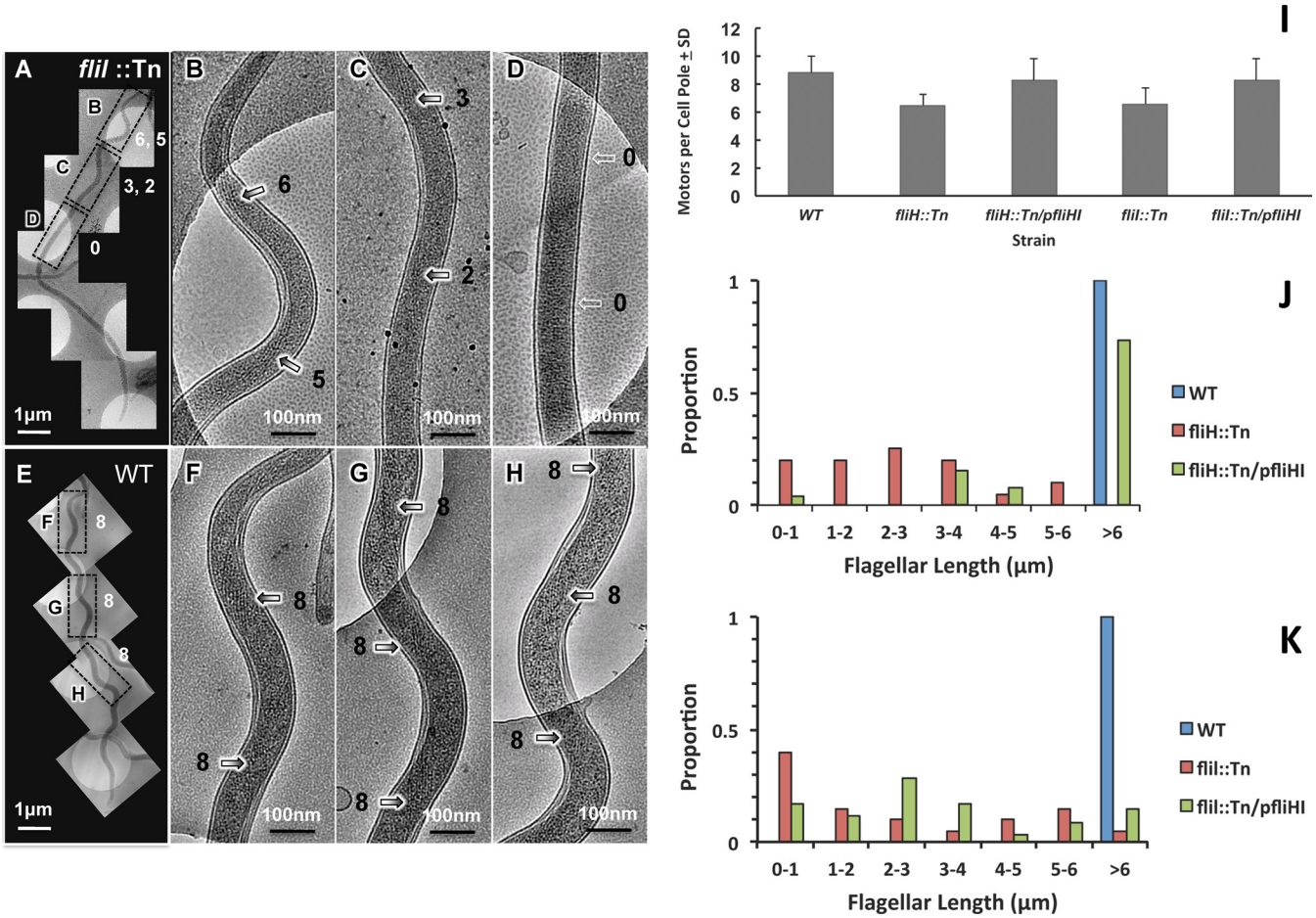

FIG 6 Reduced flagellar motor number and filament length in *fliH* and *fliI* mutants. Cryo-EM was performed at adjacent sites of representative cells, and the number of flagella and their length in all projection images were determined; examples of *fliI*::Tn mutant (A to D) and WT cells (E to H) are provided. The number of flagellar motors was restored to WT levels in complemented mutants (I). Histograms showing the lengths of flagella in WT cells, mutants, and complemented mutants were determined by cryo-EM analysis and are shown in panels J and K. Flagellar length was reduced in *fliH*::Tn and *fliI*::Tn mutant cells; length was partially restored in *fliH*::Tn/p*fliH* complemented cells (J) and to a lesser extent in *fliI*::Tn/p*fliI* cells (K).

cells were also routinely observed. In both systems, reduction in FlaB concentration was observed in mutant cells, which Guyard et al. (23) attributed to posttranslational effects, because the lack of a significant difference in *flaB* transcript levels. Overall, relatively minor differences were obtained in the *B. hermsii* and *B. burgdorferi* studies; these discrepancies may be due to the type of mutation, the methodologies employed, or true biological differences in the effects of *fliH* mutation in the two *Borrelia* species.

In conclusion, both FliH and FliI were required for the assembly of the proposed FliH-FliI complex in *B. burgdorferi*, and the absence of this complex reduced, but did not eliminate, the effective production of flagellar filaments in this organism. The formation of intact flagellar motors, hooks, and shortened flagella indicated that the FliH-FliI complex is not absolutely required for transport of rod, hook, and filament proteins by the export apparatus in this organism. However, the reduction in flagellar assembly had profound effects on spirochete motility, swimming ability in agarose matrices, morphology, cell division, and infectivity, further emphasizing the critical importance of motility in the natural infection cycle of this bacterium.

MATERIALS AND METHODS

Ethics statement. All procedures involving mice conducted at the University of Texas Health Science Center at Houston were reviewed and approved by the institutions' Animal Welfare Committee. This study was conducted in accordance with all applicable federal, state, and institutional guidelines regulating research with animals, including the PHS Policy on Humane Care and Use of Laboratory Animals, the *Guide for the Care and Use* of Laboratory Animals (60), and the United States Government Principles for the Utilization and Care of Vertebrate Animals Used in Testing, Research, and Training.

Bacterial strains and growth media. The *B. burgdorferi* strains used in this study were the *B. burgdorferi* B31 derivative 5A18NP1, its *fliH* and *fliI* mutants, and their complemented clones (Table 1). The infectious, moderately transformable clone 5A18NP1 was used for generation of *fliH* and *fliI* mutants. 5A18NP1 is a genetically engineered clone in which plasmids lp28-4 and lp56 are missing and *bbe02*, encoding a putative restriction-modification enzyme, has been disrupted (61). The *fliH* mutant T05TC243 and the *fliI* mutant T10TC009 were obtained by random, signature-tagged transposon mutagenesis using the *Himar1*-based suicide vectors pGKT-STM5 and pGKT-STM10, respectively, as described previously (22). The mutants and their complemented clones had undergone no more than three subcultures since clone isolation prior to infectivity

studies and *in vitro* phenotype characterization. The *B. burgdorferi* strains were grown in Barbour-Stoenner-Kelly II (BSKII) medium supplemented with 6% (vol/vol) rabbit serum and appropriate antibiotics or on semisolid agar plates at 34°C in 3% CO_2, as described previously (62, 63). 5A18NP1 was cultured in medium containing 200 μg/ml kanamycin, and the transposon mutants were cultured in the presence of both kanamycin and 40 μg/ml gentamicin. Additionally, streptomycin (50 μg/ml) was included in complemented transposon mutant cultures (see below). The plasmid content of each *B. burgdorferi* clone was determined using a Luminex-based procedure (64). *E. coli* TOP10, a DH5α-derived strain obtained from the Invitrogen Corporation (Carlsbad, CA), was used for the preparation of plasmids for complementation of *fliH* and *fliI* mutants.

Genetic complementation of the *fliH* and *fliI* mutants. The complementation shuttle vectors were constructed by inserting constitutive expression constructs p*flaB*::*fliH*, p*flaB*::*fliI*, and p*flaB*::*fliHI* into the shuttle vector pKFSS1 (52). Briefly, the *flaB* promoter (PflaB), the genes *fliH* and *fliI*, and the contiguous *fliHI* gene cluster were amplified by PCR using primers with engineered restriction sites (see Table S2) and were cloned into the PCR2.1 vector (Life Technologies, Grand Island, NY). PflaB was first subcloned into pKFSS1 at the SacI and KpnI sites, and then the *fliH*, *fliI*, and *fliHI* genes were fused to the 3′ end of *flaB* promoter at the KpnI site and PstI site, resulting in the complementation plasmids p*fliH*, p*fliI*, and p*fliHI*. The resultant constructs were confirmed by PCR, restriction patterns, and sequencing of PCR products. The *fliH* mutant T05TC243 and *fliI* mutant T10TC009 were transcomplemented by transforming the shuttle vectors p*fliH* and p*fliHI* into the *fliH* mutant and the shuttle vectors p*fliI* and p*fliHI* into the *fliI* mutant. As controls, parental clone 5A18NP1 was transformed with pKFSS1, p*fliH*, p*fliI*, and p*fliHI*. The *fliH* mutant T05TC243 and *fliI* mutant T10TC009 were also transformed with empty vector pKFSS1. Electroporation of *B. burgdorferi* was performed as described previously (22). All the transformants were confirmed by PCR and sequencing. The clones selected for further study are listed in Table 1.

Morphology, motility, and swimming ability studies. The morphology, motility, and swimming ability of *fliH* and *fliI* mutants, complemented clones, and the parental strain 5A18NP1 were determined in BSKII medium in the presence and absence of 1% methylcellulose under dark-field microscopy examination. Digitized photos and videos were obtained using a Nikon Eclipse microscope (Nikon, Tokyo, Japan) with Cytoviva X-cite 120 dark-field illumination (Cytoviva, Auburn, AL), a CoolSNAP HQ charge-coupled-device (CCD) camera (Photometrics, Tucson, AZ), and Nikon NIS-Elements AR3.2 software. Most of the photography and videography were performed with a 100× objective lens with an internal diaphragm (Nikon) under oil immersion.

***In vitro* growth rate measurements.** The *in vitro* growth rates of the *B. burgdorferi* B31 derivative 5A18NP1 and its *fliH* and *fliI* mutants were determined in BSKII medium. Briefly, the *B. burgdorferi* strains were grown in BSKII medium supplemented with 6% (vol/vol) rabbit serum and the appropriate antibiotics at 34°C in 3% CO_2. The concentrations of cultures were determined under dark-field microscopy examination. The spirochetes were then diluted, and the initial concentration of 5 tubes of cultures for each clone was adjusted to 10^4 cells per ml. We determined the concentrations of *B. burgdorferi* cultures over 11 days. A chain of string-like *fliH* or *fliI* mutant cells was counted as one spirochete.

Swarm plate assay. The medium for the swarm plate assays was prepared by mixing 205.2 ml plating BSK (P-BSK) medium (63) with 10.2 ml of rabbit serum, prewarming the P-BSK–rabbit serum mixture at 50°C, and adding 25.7 ml of softened 1.7% agarose to 149.3 ml of the prewarmed mixture to make 0.25% agarose plates. After mixing, 35 ml of the mixture was transferred into 100-mm petri plates. The *fliH* and *fliI* mutants, their parental clone 5A18NP1, and the complemented clones were cultured directly from frozen stocks in BSKII medium to late log phase. The cells were harvested by centrifugation, the pellet was resuspended in phosphate-buffered saline (PBS), and the *B. burgdorferi* concentration was adjusted to 1×10^9 cells/ml. Ten microliters of the suspensions (1×10^7 organisms) was added in 2-mm punch wells in the plates. The plates were incubated at 37°C with 3% CO_2 for 3 to 5 days, and the diameter of the translucent "halo" was determined. Four replicate plates were used in each assay.

Protein profiles and Western blot analysis. SDS-PAGE with Coomassie brilliant blue staining and Western blot analysis of *fliH* and *fliI* mutants and their parental strain 5A18NP1 were performed as described previously (22). Mouse monoclonal anti-FlaB antibody H9724 followed by a goat anti-mouse IgG-horseradish peroxidase conjugate and chemiluminescence reagents were utilized for immunostaining.

RT-PCR analysis of genes downstream of *fliH* and *fliI*. RNA was isolated from *B. burgdorferi* B31 parental clone 5A18NP1 and its *fliH* and *fliI* mutants in BSKII medium to mid-log phase using RNAprotect bacterial reagent and an RNeasy minikit (Qiagen, Valencia, CA, USA), as indicated above. The resulting RNA preparations were treated with the Turbo DNA-free kit (Ambion, Austin, TX) according to the manufacturer's recommendations to reduce possible contamination with genomic DNA. The RNA samples were then quantitated by UV spectroscopy and examined by agarose gel electrophoresis. Reverse transcription was performed at 50°C for 30 min using 200 ng of RNA and primers specific to *fliH* downstream genes *fliI* and *fliJ* (also called *flbA*) (see Table S2) by following the protocol of the Qiagen OneStep RT-PCR kit (Qiagen, Valencia, CA, USA). Subsequent PCRs were performed in volumes of 50 μl containing 10 μl of 5× Qiagen OneStep RT-PCR buffer, 2 μl of 10 mM each deoxynucleoside triphosphate (dNTPs), 3 μl of 10 μM primers, and 2 μl of Qiagen OneStep RT-PCR enzyme mix. PCRs were performed in an Eppendorf Mastercycler thermocycler (Foster City, CA, United States), using the following conditions: 95°C for 2 min followed by 35 cycles of (i) denaturation at 94°C for 1 min, (ii) annealing at 52°C for 30 s, and (iii) extension at 72°C for 1 min and a final extension at 72°C for 10 min. Products were examined by agarose gel electrophoresis and ethidium bromide staining. Quantitative RT-PCR was carried out in triplicate using 10 ng samples of cDNA per reaction. Amplification was carried out using a C1000Touch/CFX96 real-time system (Bio-Rad, Hercules, CA), iQ SYBR green supermix (Bio-Rad), and primers specific for *fliI*, *fliJ*, *flaB*, and control gene *BB0337* (enolase) (see Table S2). qPCR was performed as follows: 95°C for 3 min and 40 cycles of 95°C for 10 s followed by 60°C for 30 s. Standard curves were generated for each primer pair by diluting a known quantity of genomic DNA in a series of 10-fold serial dilutions. Threshold cycle values were plotted to determine quantities of each target. Melting curve analyses were performed to assess the presence of single products. Results were analyzed using CFX Manager software (Bio-Rad, Hercules, CA). Expression levels based on quantification cycle (C_q) values were normalized first to the corresponding *BB0337* values and then to the 5A18NP1 parental control for each gene of interest.

Mouse infection studies. Infectivity of *B. burgdorferi* B31 clone 5A18NP1 and its *fliH* and *fliI* mutants was previously screened using a signature-tagged mutagenesis procedure and high-throughput semiquantitative Luminex FlexMap technology (22). In this study, infectivity of the mutants and complemented clones was further examined by single clone inoculation. Briefly, the concentration of spirochetes was determined by dark-field microscopy, and groups of 6 mice were inoculated with 1×10^5 organisms for each clone subcutaneously at the base of the tail as described previously (57). Blood was collected for culture of organisms on day 7 postinoculation. Groups of 3 mice were sacrificed at days 14 and 28 postinoculation, and skin, ear, tibiotarsal joint, heart, and urinary bladder were collected. The tissue specimens were cultured in 2 ml BSKII medium containing kanamycin and gentamicin for *fliH* and *fliI* mutants and kanamycin, gentamicin, and streptomycin for complemented clones of *fliH* and *fliI* mutants. Cultures were examined by dark-field microscopy at 3- to 4-day intervals over a 3-week period for the presence of *B. burgdorferi* organisms.

Cryo-electron tomography and subvolume averaging. The *B. burgdorferi* B31 clone 5A18NP1, its *fliH* and *fliI* mutants, and their complementation clones were cultured directly from frozen stocks in BSKII medium to mid-log phase. Two milliliters of each *B. burgdorferi* culture was

centrifuged at 5,000 × *g* for 5 min, and the resulting pellet was rinsed 2 times with 1 ml PBS at 3,000 × *g* for 1 min. The final pellet was resuspended in 30 μl PBS. The specimens were mixed with 15-nm colloidal fiducial gold markers and then deposited onto freshly glow-discharged holey carbon grids. The grids were blotted with filter paper and then rapidly frozen in liquid ethane. Specimens were imaged at −170°C using a 300-kV Polara G2 electron microscope (FEI) with a field emission gun and a 16-megapixel CCD camera (TVIPS). Low-dose, single-axis tilt series were collected from to −64° to +64° with an angular increment of 2° using the FEI batch tomography program. Three-dimensional flagellar motor models were constructed by collecting the tilt series from cell poles at 31,000× and ~8-μm defocus with a cumulative dose of ~100 e^{-}/Å^2 distributed over 65 images. The effective pixel size was 5.7 Å after 2-by-2 binning. A total of 303 tomographic reconstructions were generated, and 1,626 flagellar motor subvolumes were extracted from *fliH* and *fliI* mutants and their complemented clones (see Table S1 in the supplemental material). The subvolumes (256 by 256 by 256 voxels) of the flagellar motors of each clone were aligned as previously described (11, 12). The flagellar motor number in each cell tip was determined by collecting the tilt series at a lower magnification of ×9,400 and reconstructing a total of 45 cell tomograms from WT 5A18NP1, its *fliH* and *fliI* mutants, and their complemented clones (see Table S1). Tilt series were automatically aligned and reconstructed using a combination of IMOD (65) and RAPTOR (66).

Cryo-electron microscopy. The morphology and flagellar length of the spirochete were examined by acquiring cryo-EM images with the Polara G2 electron microscope and a K2 summit (Gatan) direct detection camera. The field of view covers ~3 μm of cell length at a magnification of ×4,700 (pixel size, ~8 Å). Four to seven images were montaged to build a whole-cell image. Dose fractionation mode was used to acquire two-dimensional (2D) projection images. Each single image was split into 20 frames during acquisition. The stack of 20 frames were aligned and drift-corrected using xfalign (65) and then averaged to enhance the image quality. A total of 336 dose-fractionated projection images were acquired, and ~60 whole cells were imaged.

SUPPLEMENTAL MATERIAL

Supplemental material for this article may be found at http://mbio.asm.org/lookup/suppl/doi:10.1128/mBio.00579-15/-/DCSupplemental.

Figure S1, TIF file, 0.4 MB.
Figure S2, TIF file, 0.7 MB.
Figure S3, TIF file, 2.8 MB.
Table S1, PDF file, 0.04 MB.
Table S2, PDF file, 0.01 MB.
Movie S1, MOV file, 9.2 MB.
Movie S2, MOV file, 1.4 MB.
Movie S3, MOV file, 9.9 MB.
Movie S4, MOV file, 2.2 MB.
Movie S5, MOV file, 2.1 MB.

ACKNOWLEDGMENTS

Research reported in this publication was supported by the National Institute of Allergy and Infectious Diseases of the National Institutes of Health under award numbers R01AI059048 (S.J.N. and T.L.) and R01AI087946 (J.L. and S.J.N.) and by the Welch Foundation under award no. AU-1714 (J.L.).

The content is solely the responsibility of the authors and does not necessarily represent the official views of the National Institutes of Health or the Welch Foundation.

REFERENCES

1. **Steere AC, Coburn J, Glickstein L.** 2004. The emergence of Lyme disease. J Clin Invest **113:**1093–1101. http://dx.doi.org/10.1172/JCI21681.
2. **Samuels DS, Radolf JD.** 2010. *Borrelia*: molecular biology, host interaction and pathogenesis. Caister Academic Press, Hethersett, Norwich, United Kingdom.
3. **Lane RS, Piesman J, Burgdorfer W.** 1991. Lyme borreliosis: relation of its causative agent to its vectors and hosts in North America and Europe. Annu Rev Entomol **36:**587–609. http://dx.doi.org/10.1146/annurev.en.36.010191.003103.
4. **Norris SJ, Coburn J, Leong JM, Hu LT, Höök M.** 2010. Pathobiology of Lyme disease *Borrelia*, p 299–331. In Samuels DS, Radolf JD (ed), *Borrelia*: molecular and cellular biology. Caister Academic Press, Hethersett, Norwich, United Kingdom.
5. **Steere AC, Sikand VK.** 2003. The presenting manifestations of Lyme disease and the outcomes of treatment. N Engl J Med **348:**2472–2474. http://dx.doi.org/10.1056/NEJM200306123482423.
6. **Stanek G, Strle F.** 2003. Lyme borreliosis. Lancet **362:**1639–1647. http://dx.doi.org/10.1016/S0140-6736(03)14798-8.
7. **Kimsey RB, Spielman A.** 1990. Motility of Lyme disease spirochetes in fluids as viscous as the extracellular matrix. J Infect Dis **162:**1205–1208. http://dx.doi.org/10.1093/infdis/162.5.1205.
8. **Charon NW, Cockburn A, Li C, Liu J, Miller KA, Miller MR, Motaleb MA, Wolgemuth CW.** 2012. The unique paradigm of spirochete motility and chemotaxis. Annu Rev Microbiol **66:**349–370. http://dx.doi.org/10.1146/annurev-micro-092611-150145.
9. **Charon NW, Goldstein SF, Marko M, Hsieh C, Gebhardt LL, Motaleb MA, Wolgemuth CW, Limberger RJ, Rowe N.** 2009. The flat-ribbon configuration of the periplasmic flagella of *Borrelia burgdorferi* and its relationship to motility and morphology. J Bacteriol **191:**600–607. http://dx.doi.org/10.1128/JB.01288-08.
10. **Fraser CM, Casjens S, Huang WM, Sutton GG, Clayton R, Lathigra R, White O, Ketchum KA, Dodson R, Hickey EK, Gwinn M, Dougherty B, Tomb JF, Fleischmann RD, Richardson D, Peterson J, Kerlavage AR, Quackenbush J, Salzberg S, Hanson M, van Vugt R, Palmer N, Adams MD, Gocayne J, Weidman J, Utterback T, Watthey L, McDonald L, Artiach P, Bowman C, Garland S, Fujii C, Cotton MD, Horst K, Roberts K, Hatch B, Smith HO, Venter JC.** 1997. Genomic sequence of a Lyme disease spirochaete, *Borrelia burgdorferi*. Nature **390:**580–586. http://dx.doi.org/10.1038/37551.
11. **Zhao X, Zhang K, Boquoi T, Hu B, Motaleb MA, Miller KA, James ME, Charon NW, Manson MD, Norris SJ, Li C, Liu J.** 2013. Cryoelectron tomography reveals the sequential assembly of bacterial flagella in *Borrelia burgdorferi*. Proc Natl Acad Sci U S A **110:**14390–14395. http://dx.doi.org/10.1073/pnas.1308306110.
12. **Liu J, Lin T, Botkin DJ, McCrum E, Winkler H, Norris SJ.** 2009. Intact flagellar motor of *Borrelia burgdorferi* revealed by cryo-electron tomography: evidence for stator ring curvature and rotor/C-ring assembly flexion. J Bacteriol **191:**5026–5036. http://dx.doi.org/10.1128/JB.00340-09.
13. **Chen S, Beeby M, Murphy GE, Leadbetter JR, Hendrixson DR, Briegel A, Li Z, Shi J, Tocheva EI, Müller A, Dobro MJ, Jensen GJ.** 2011. Structural diversity of bacterial flagellar motors. EMBO J **30:**2972–2981. http://dx.doi.org/10.1038/emboj.2011.186.
14. **Murphy GE, Leadbetter JR, Jensen GJ.** 2006. *In situ* structure of the complete *Treponema primitia* flagellar motor. Nature **442:**1062–1064. http://dx.doi.org/10.1038/nature05015.
15. **Raddi G, Morado DR, Yan J, Haake DA, Yang XF, Liu J.** 2012. Three-dimensional structures of pathogenic and saprophytic *Leptospira* species revealed by cryo-electron tomography. J Bacteriol **194:**1299–1306. http://dx.doi.org/10.1128/JB.06474-11.
16. **Zhao X, Norris SJ, Liu J.** 2014. Molecular architecture of the bacterial flagellar motor in cells. Biochemistry **53:**4323–4333. http://dx.doi.org/10.1021/bi500059y.
17. **Macnab RM.** 2003. How bacteria assemble flagella. Annu Rev Microbiol **57:**77–100. http://dx.doi.org/10.1146/annurev.micro.57.030502.090832.
18. **Chevance FF, Hughes KT.** 2008. Coordinating assembly of a bacterial macromolecular machine. Nat Rev Microbiol **6:**455–465. http://dx.doi.org/10.1038/nrmicro1887.
19. **Liu J, Howell JK, Bradley SD, Zheng Y, Zhou ZH, Norris SJ.** 2010. Cellular architecture of *Treponema pallidum*: novel flagellum, periplasmic cone, and cell envelope as revealed by cryo electron tomography. J Mol Biol **403:**546–561. http://dx.doi.org/10.1016/j.jmb.2010.09.020.
20. **Motaleb MA, Corum L, Bono JL, Elias AF, Rosa P, Samuels DS, Charon NW.** 2000. *Borrelia burgdorferi* periplasmic flagella have both skeletal and motility functions. Proc Natl Acad Sci U S A **97:**10899–10904. http://dx.doi.org/10.1073/pnas.200221797.
21. **Li C, Xu H, Zhang K, Liang FT.** 2010. Inactivation of a putative flagellar motor switch protein FliG1 prevents *Borrelia burgdorferi* from swimming in highly viscous media and blocks its infectivity. Mol Mi-

crobiol **75:**1563–1576. http://dx.doi.org/10.1111/j.1365-2958.2010.07078.x.

22. **Lin T, Gao L, Zhang C, Odeh E, Jacobs MB, Coutte Lc, Chaconas G, Philipp MT, Norris SJ.** 2012. Analysis of an ordered, comprehensive STM mutant library in infectious *Borrelia burgdorferi*: insights into the genes required for mouse infectivity. PLoS One **7:**e47532. http://dx.doi.org/10.1371/journal.pone.0047532.
23. **Guyard C, Raffel SJ, Schrumpf ME, Dahlstrom E, Sturdevant D, Ricklefs SM, Martens C, Hayes SF, Fischer ER, Hansen BT, Porcella SF, Schwan TG.** 2013. Periplasmic flagellar export apparatus protein, FliH, is involved in post-transcriptional regulation of FlaB, motility and virulence of the relapsing fever spirochete *Borrelia hermsii*. PLoS One **8:**e72550. http://dx.doi.org/10.1371/journal.pone.0072550.
24. **Sultan SZ, Manne A, Stewart PE, Bestor A, Rosa PA, Charon NW, Motaleb MA.** 2013. Motility is crucial for the infectious life cycle of *Borrelia burgdorferi*. Infect Immun **81:**2012–2021. http://dx.doi.org/10.1128/IAI.01228-12.
25. **Berg HC.** 2003. The rotary motor of bacterial flagella. Annu Rev Biochem **72:**19–54. http://dx.doi.org/10.1146/annurev.biochem.72.121801.161737.
26. **Minamino T.** 2014. Protein export through the bacterial flagellar type III export pathway. Biochim Biophys Acta **1843:**1642–1648. http://dx.doi.org/10.1016/j.bbamcr.2013.09.005.
27. **Blocker A, Komoriya K, Aizawa S.** 2003. Type III secretion systems and bacterial flagella: insights into their function from structural similarities. Proc Natl Acad Sci U S A **100:**3027–3030. http://dx.doi.org/10.1073/pnas.0535335100.
28. **Paul K, Erhardt M, Hirano T, Blair DF, Hughes KT.** 2008. Energy source of flagellar type III secretion. Nature **451:**489–492. http://dx.doi.org/10.1038/nature06497.
29. **Cornelis GR.** 2006. The type III secretion injectisome. Nat Rev Micro **4:**811–825. http://dx.doi.org/10.1038/nrmicro1526.
30. **Minamino T, Macnab RM.** 1999. Components of the *Salmonella* flagellar export apparatus and classification of export substrates. J Bacteriol **181:**1388–1394.
31. **Minamino T, Namba K.** 2008. Distinct roles of the FliI ATPase and proton motive force in bacterial flagellar protein export. Nature **451:**485–488. http://dx.doi.org/10.1038/nature06449.
32. **Minamino T, Yoshimura SD, Morimoto YV, González-Pedrajo B, Kami-ike N, Namba K.** 2009. Roles of the extreme N-terminal region of FliH for efficient localization of the FliH–FliI complex to the bacterial flagellar type III export apparatus. Mol Microbiol **74:**1471–1483. http://dx.doi.org/10.1111/j.1365-2958.2009.06946.x.
33. **Claret L, Calder SR, Higgins M, Hughes C.** 2003. Oligomerization and activation of the FliI ATPase central to bacterial flagellum assembly. Mol Microbiol **48:**1349–1355. http://dx.doi.org/10.1046/j.1365-2958.2003.03506.x.
34. **Minamino T, Kazetani K, Tahara A, Suzuki H, Furukawa Y, Kihara M, Namba K.** 2006. Oligomerization of the bacterial flagellar ATPase FliI is controlled by its extreme N-terminal region. J Mol Biol **360:**510–519. http://dx.doi.org/10.1016/j.jmb.2006.05.010.
35. **Koonin EV.** 1993. A common set of conserved motifs in a vast variety of putative nucleic acid-dependent ATPases including MCM proteins involved in the initiation of eukaryotic DNA replication. Nucleic Acids Res **21:**2541–2547. http://dx.doi.org/10.1093/nar/21.11.2541.
36. **Vogler AP, Homma M, Irikura VM, Macnab RM.** 1991. *Salmonella typhimurium* mutants defective in flagellar filament regrowth and sequence similarity of FliI to F0F1, vacuolar, and archaebacterial ATPase subunits. J Bacteriol **173:**3564–3572.
37. **Lane MC, O'Toole PW, Moore SA.** 2006. Molecular basis of the interaction between the flagellar export proteins FliI and FliH from *Helicobacter pylori*. J Biol Chem **281:**508–517. http://dx.doi.org/10.1074/jbc.M507238200.
38. **Imada K, Minamino T, Tahara A, Namba K.** 2007. Structural similarity between the flagellar type III ATPase FliI and F1-ATPase subunits. Proc Natl Acad Sci U S A **104:**485–490. http://dx.doi.org/10.1073/pnas.0608090104.
39. **Fan F, Macnab RM.** 1996. Enzymatic characterization of FliI: an ATPase involved in flagellar assembly in assembly in *Salmonella typhimurium*. J Biol Chem **271:**31981–31988. http://dx.doi.org/10.1074/jbc.271.50.31981.
40. **Miwa K, Yoshida M.** 1989. The alpha 3 beta 3 complex, the catalytic core of F1-ATPase. Proc Natl Acad Sci U S A **86:**6484–6487. http://dx.doi.org/10.1073/pnas.86.17.6484.
41. **Erhardt M, Mertens ME, Fabiani FD, Hughes KT.** 2014. ATPase-independent type-III protein secretion in *Salmonella enterica*. PLoS Genet **10:**e1004800. http://dx.doi.org/10.1371/journal.pgen.1004800.
42. **Ibuki T, Imada K, Minamino T, Kato T, Miyata T, Namba K.** 2011. Common architecture of the flagellar type III protein export apparatus and F- and V-type ATPases. Nat Struct Mol Biol **18:**277–282. http://dx.doi.org/10.1038/nsmb.1977.
43. **Fraser GM, González-Pedrajo B, Macnab RM.** 2003. Interactions of FliJ with the *Salmonella* type III flagellar export apparatus. J Bacteriol **185:**5546–5554. http://dx.doi.org/10.1128/JB.185.18.5546-5554.2003.
44. **Minamino T, Macnab RM.** 2000. FliH, a soluble component of the type III flagellar export apparatus of *Salmonella*, forms a complex with FliI and inhibits its ATPase activity. Mol Microbiol **37:**1494–1503. http://dx.doi.org/10.1046/j.1365-2958.2000.02106.x.
45. **Minamino T, González-Pedrajo B, Kihara M, Namba K, Macnab RM.** 2003. The ATPase FliI can interact with the type III flagellar protein export apparatus in the absence of its regulator, FliH. J Bacteriol **185:**3983–3988. http://dx.doi.org/10.1128/JB.185.13.3983-3988.2003.
46. **González-Pedrajo B, Fraser GM, Minamino T, Macnab RM.** 2002. Molecular dissection of *Salmonella* FliH, a regulator of the ATPase FliI and the type III flagellar protein export pathway. Mol Microbiol **45:**967–982. http://dx.doi.org/10.1046/j.1365-2958.2002.03047.x.
47. **Minamino T, Macnab RM.** 2000. Interactions among components of the *Salmonella* flagellar export apparatus and its substrates. Mol Microbiol **35:**1052–1064. http://dx.doi.org/10.1046/j.1365-2958.2000.01771.x.
48. **Minamino T, Chu R, Yamaguchi S, Macnab RM.** 2000. Role of FliJ in flagellar protein export in *Salmonella*. J Bacteriol **182:**4207–4215. http://dx.doi.org/10.1128/JB.182.15.4207-4215.2000.
49. **Bange G, Kümmerer N, Engel C, Bozkurt G, Wild K, Sinning I.** 2010. FlhA provides the adaptor for coordinated delivery of late flagella building blocks to the type III secretion system. Proc Natl Acad Sci U S A **107:**11295–11300. http://dx.doi.org/10.1073/pnas.1001383107.
50. **Evans LD, Stafford GP, Ahmed S, Fraser GM, Hughes C.** 2006. An escort mechanism for cycling of export chaperones during flagellum assembly. Proc Natl Acad Sci U S A **103:**17474–17479. http://dx.doi.org/10.1073/pnas.0605197103.
51. **Imada K, Minamino T, Kinoshita M, Furukawa Y, Namba K.** 2010. Structural insight into the regulatory mechanisms of interactions of the flagellar type III chaperone FliT with its binding partners. Proc Natl Acad Sci U S A **107:**8812–8817. http://dx.doi.org/10.1073/pnas.1001866107.
52. **Frank KL, Bundle SF, Kresge ME, Eggers CH, Samuels DS.** 2003. *aadA* confers streptomycin resistance in *Borrelia burgdorferi*. J Bacteriol **185:**6723–6727. http://dx.doi.org/10.1128/JB.185.22.6723-6727.2003.
53. **Macnab RM.** 2004. Type III flagellar protein export and flagellar assembly. Biochim Biophys Acta **1694:**207–217. http://dx.doi.org/10.1016/j.bbamcr.2004.04.005.
54. **González-Pedrajo B, Minamino T, Kihara M, Namba K.** 2006. Interactions between C ring proteins and export apparatus components: a possible mechanism for facilitating type III protein export. Mol Microbiol **60:**984–998. http://dx.doi.org/10.1111/j.1365-2958.2006.05149.x.
55. **McMurry JL, Murphy JW, González-Pedrajo B.** 2006. The FliN-FliH interaction mediates localization of flagellar export ATPase FliI to the C ring complex. Biochemistry **45:**11790–11798. http://dx.doi.org/10.1021/bi0605890.
56. **Botkin DJ, Abbott AN, Stewart PE, Rosa PA, Kawabata H, Watanabe H, Norris SJ.** 2006. Identification of potential virulence determinants by *Himar1* transposition of infectious *Borrelia burgdorferi* B31. Infect Immun **74:**6690–6699. http://dx.doi.org/10.1128/IAI.00993-06.
57. **Lin T, Gao L, Edmondson DG, Jacobs MB, Philipp MT, Norris SJ.** 2009. Central role of the Holliday junction helicase RuvAB in *vlsE* recombination and infectivity of *Borrelia burgdorferi*. PLoS Pathog **5:**e1000679. http://dx.doi.org/10.1371/journal.ppat.1000679.
58. **Hübner A, Yang X, Nolen DM, Popova TG, Cabello FC, Norgard MV.** 2001. Expression of *Borrelia burgdorferi* OspC and DbpA is controlled by a RpoN-RpoS regulatory pathway. Proc Natl Acad Sci U S A **98:**12724–12729. http://dx.doi.org/10.1073/pnas.231442498.
59. **Sartakova ML, Dobrikova EY, Motaleb MA, Godfrey HP, Charon NW, Cabello FC.** 2001. Complementation of a nonmotile *flaB* mutant of *Borrelia burgdorferi* by chromosomal integration of a plasmid containing a wild-type *flaB* allele. J Bacteriol **183:**6558–6564. http://dx.doi.org/10.1128/JB.183.22.6558-6564.2001.
60. **National Research Council.** 2011. Guide for the care and use of laboratory animals, 8th ed. National Academies Press, Washington, DC.
61. **Kawabata H, Norris SJ, Watanabe H.** 2004. BBE02 disruption mutants of *Borrelia burgdorferi* B31 have a highly transformable, infectious pheno-

type. Infect Immun **72:**7147–7154. http://dx.doi.org/10.1128/IAI.72.12.7147-7154.2004.
62. **Barbour AG**. 1984. Isolation and cultivation of Lyme disease spirochetes. Yale J Biol Med **57:**521–525.
63. **Norris SJ, Howell JK, Garza SA, Ferdows MS, Barbour AG**. 1995. High- and low-infectivity phenotypes of clonal populations of *in vitro*-cultured *Borrelia burgdorferi*. Infect Immun **63:**2206–2212.
64. **Norris SJ, Howell JK, Odeh EA, Lin T, Gao L, Edmondson DG**. 2011. High-throughput plasmid content analysis of *Borrelia burgdorferi* B31 by using Luminex multiplex technology. Appl Environ Microbiol **77:**1483–1492. http://dx.doi.org/10.1128/AEM.01877-10.
65. **Kremer JR, Mastronarde DN, McIntosh JR**. 1996. Computer visualization of three-dimensional image data using IMOD. J Struct Biol **116:**71–76. http://dx.doi.org/10.1006/jsbi.1996.0013.
66. **Amat F, Moussavi F, Comolli LR, Elidan G, Downing KH, Horowitz M**. 2008. Markov random field based automatic image alignment for electron tomography. J Struct Biol **161:**260–275. http://dx.doi.org/10.1016/j.jsb.2007.07.007.